International Research Journal of Innovations in Engineering and Technology (IRJIET)

ISSN (online): 2581-3048

Volume 6, Issue 3, pp 13-23, March-2022

https://doi.org/10.47001/IRJIET/2022.603003

Three Dimensional CFD of Supercritical CO_2 Flow Characterization in a Centrifugal Compressor

[1]Firas Khaleel Hussein Alok, [2]Dr. Younis M. Najim

[1,2]University of Mosul, Mosul, Iraq

Authors Email: [1]firas.enp70@student.uomosul.edu.iq [2]mahalyounis@uomosul.edu.iq

Abstract **- Research and development on the supercritical Brayton power cycle has been powered by its higher thermal efficiency, component compactness, lower corrosiveness, and emission. Modeling of the supercritical fluid flow in a centrifugal compressor passage involves difficulties such as complicated domain, high turbulent intensity, viscus, and unsteady operation in a rotating frame of reference. Furthermore, the variation of supercritical thermophysical requires a robust model to account for real gas behavior. In this work, CFD of three-dimensional Reynolds Averaged Navier-Stokes (RANS) equations are solved to reproduce the flow structure, pressure, and temperature evolution in the centrifugal passages. The Menter turbulence model is used to address the RANS closure problem. The fluid properties are modelled by coupling the CFD solver with the REFPROP database. The Sandia impeller is used in this work to validate the CFD results. Twelve cases of different operating conditions are considered in this work to study the performance of supercritical CO_2 centrifugal compressor. The validation results conclude that there is good agreement with the experimental data. The CFD results reveal that the flow velocity varies from 17.9 to 138 m/s as the impeller speed changes from 10000 to 64900 rpm. The flow velocity accelerates faster on the suction side than on the pressure side of both splitter and main blade. Vortical flow is seen behind the trailing edge of vaned diffuser blades due to relatively thick blade at the trailing edge. The tip clearance and secondary flow disturbs the flow at span 90% and intensify the turbulence in the flow. The results also reveal the nonlinear variation of the real fluid thermophysical properties. This behavior imposes considerable challenges to CFD analysis of the centrifugal compressor where the SCO_2 density approaches 60% of the water density while fluid being compressed to a pressure ratio up to 1.5.**

Keywords: Three Dimensional CFD, CO2, Flow Characterization, Centrifugal Compressor.

1. Introduction

Unlike conventional power cycles that use steam as the working fluid to generate power, the supercritical carbon dioxide Brayton power cycles use carbon dioxide at a working temperature and pressure above its critical point. The supercritical CO_2 Brayton power cycles have the following advantages: (1) higher thermal efficiency up to 50% compared to conventional steam cycles, (2) high-pressure SCO_2 cycles produce a high-density working fluid, which could lead to smaller equipment sizes and plant footprints, and thus lower capital costs[1], (3) reliable scalability of power output (from 1MW to > 100MW);(4) CO_2 is a corrosion inhibitor and produces lower corrosion for the cycle component, which reduces the material requirement and allows higher working temperatures compared with conventional steam power plants [2]–[4], and(5) Lowering fuel costs, reducing water usage, and lowering emissions from fossil fuel heat sources are all advantages of increased cycle efficiency[1]. The centrifugal compressor is a key component in the Brayton power cycle that is used to raise the pressure of the supercritical CO_2 prior to heat addition to the fluid. The supercritical CO_2 centrifugal compressor experiences several challenges represented by the rapid variation in fluid properties such as density, specific heat ratio, and low gas compressibility factor, which makes the traditional ideal gas analysis unable to predict the performance of the compressor. Therefore, the design of the supercritical compressor is undergoing intensive research and development to provide a reliable and constant efficiency compressor. Motoaki et al. (2011)[5]have examined the aerodynamic characteristics of a centrifugal compressor in a closed-cycle gas turbine using supercritical carbon dioxide as a working fluid. The experiment shows that the compressor performance improved when the compressibility factor decreased.Enrico et al. (2013) [6] have introduced a methodology for the aerodynamic design of a compressor in power plant units that operates on supercritical carbon dioxide and compared it with the Sandia National Laboratory (SNL) [7] radial compressor. The results showed that the flow field exhibits a smooth variation of the thermodynamic properties through the impeller passage. The compressor efficiency was estimated to be 62.5 percent, and the pressure ratio was 1.1.The comparison between calculated efficiency and ideal head

International Research Journal of Innovations in Engineering and Technology (IRJIET)

ISSN (online): 2581-3048

Volume 6, Issue 3, pp 13-23, March-2022

https://doi.org/10.47001/IRJIET/2022.603003

coefficient with the experimental data showed differences of about 4% and 25%, respectively. Zhao et al., 2014 [8] have theoretically studied a single-stage centrifugal compressor with a vaneless and vaned diffuser. The compressor uses carbon dioxide as a working fluid with an inlet operating condition just above the critical point. NNUMECA/Turbo coupled with NIST REFPROP was used to solve the three-dimensional CFD problem. The impeller has nine main blades and nine splitter blades, and the outlet radius is 170 mm. It was observed that no low pressure region developed near the leading edge of the vaned diffuser. It was noted that the vaneless diffuser improves the performance of the compressor regarding aerodynamic characteristics. The vaneless diffuser was in order to control and reduce the difference in fluid distribution and avoid low pressure regions by increasing the static pressure for the working fluid. It was concluded that the regions of low pressure are in the locations at the leading edge of the section side and at the edges of the corners of the trailing edge of the rotor blades, and adding the vaneless diffuser works to weaken these regions, so the vaneless diffuser can improve the performance of the compressor. Alireza Ameli1 et al. (2018) [9]used individual enthalpy loss models to design and simulate the centrifugal compressor. Due to the small size of the compressor and high density near the critical point, the friction loss was found to play a noticeable role among the internal enthalpy loss models. A comparison was made between different friction loss models and a general correlation between friction loss and friction factor was derived. The obtained results were verified against experimental measurements from the SNL[7] and time-dependent CFD simulations. In 2018, another study by Raman and Kim [10] investigated the performance of the SCO_2 Sandia radial compressor using supercritical CO_2, which was considered an ideal gas. The influence of individual components on the performance characteristics was studied and analyzed. It was suggested that the vaneless diffuser reduces the risk of phase transition by decreasing the pressure drop below inlet conditions. Li et al. (2020)[11] have examined the CFD analysis of a centrifugal compressor using supercritical CO_2 to increase the swallowing capacity at the impeller inlet. This study uses CFD scheme to study the flow structure in SNL [7]for supercritical CO_2 centrifugal compressor.

2. Numerical Modeling

The modelling of the supercritical fluid flow in a centrifugal compressor passage involves difficulties due to: (1) complicated geometry, which imposes changes in the discretization of the computational domain; (2) high turbulent intensity; (3) viscos and unsteady under rotating frame of reference and (4) variation of supercritical thermophysical properties is inventible and ideal gas assumption is no longer valid. Three dimensional Reynolds Averaged Navier-Stokes (RANS) equations are solved to reproduce the flow structure, pressure, and temperature evolution in the centrifugal passages. The Menter turbulence model is used to address the RANS closure problem[12]. The fluid properties are recalled by coupling the CFD solver with the REFPROP database to accurately model the real gas behavior. The 3D-RANS equation can be written as[13]:

The continuity equation in rotating frame of reference:

$$\frac{\partial \rho}{\partial t} + \frac{\partial}{\partial x_j}(\rho u_j) = 0 \qquad (1)$$

The momentum equation in rotating frame of reference:

$$\frac{\partial}{\partial t}(\rho u_j) + \frac{\partial}{\partial x_j}(\rho u_j u_i) = -\frac{\partial p}{\partial x_i} + \frac{\partial}{\partial x_j}\left\{\mu_{eff}\left(\frac{\partial u_i}{\partial x_j} + \frac{\partial u_j}{\partial x_i}\right)\right\} + \boldsymbol{S}_{ui} \quad (2)$$

The energy equation in rotating frame of reference:

$$\frac{\partial}{\partial t}(\rho I) - \frac{\partial P}{\partial t} + \frac{\partial}{\partial x_j}(\rho u_j I) = \frac{\partial}{\partial x_j}\left(\lambda \frac{\partial T}{\partial x_j} + \frac{\mu_t}{\mathrm{Pr_t}}\frac{\partial I}{\partial x_i}\right) + \frac{\partial}{\partial x_j}\left\{u_i\left[\mu_t\left(\frac{\partial u_i}{\partial x_j} + \frac{\partial u_j}{\partial x_i}\right) - \frac{2}{3}\mu_t \frac{\partial u_i}{\partial x_i}\delta_{ij}\right]\right\} \qquad (3)$$

Where $\mu_{eff} = \mu + \mu_t$. And here, $\boldsymbol{S}_{ui}$ is a momentum source account for the rotating frame of reference which includes effects of both the Coriolis force ($\vec{\mathbf{S}}_{\mathrm{Cor}}$) and the centrifugal force ($\vec{\mathbf{S}}_{\mathrm{cfg}}$) such as:

$$\vec{S}_{ui} = \vec{S}_{Cor} + \vec{S}_{cfg} \qquad (4)$$

Both the Coriolis force ($\vec{\mathbf{S}}_{\mathrm{Cor}}$) and the centrifugal force ($\vec{\mathbf{S}}_{\mathrm{cfg}}$), are shown as follow:

$$\vec{\mathbf{S}}_{\mathrm{Cor}} = -2\rho\vec{\Omega} \times \vec{\mathbf{U}} \qquad (5)$$

$$\vec{\mathbf{S}}_{\mathrm{cfg}} = -\rho\vec{\Omega} \times (\vec{\Omega} \times \vec{\mathbf{r}}) \qquad (6)$$

Here, **r** is the location vector and **U** is the relative frame velocity (that is, the rotating frame velocity for a rotating frame of reference).

It should be mentioned that steady state analysis is used in this work, hence the transient terms should be canceled.

Grid independence test

A Mesh independent study is a common tool used to ensure that the mesh size is enough to capture the physics variation and validate linearization over a computational cell, also called an Eulerian cube. The thermodynamic equilibrium must be held in a computational cell to apply the energy equation, or first law of thermodynamics. An independent test was conducted, and the result concluded that no variation

International Research Journal of Innovations in Engineering and Technology (IRJIET)

ISSN (online): 2581-3048

Volume 6, Issue 3, pp 13-23, March-2022

https://doi.org/10.47001/IRJIET/2022.603003

could be seen when the computational domain is discretized into 1.2 million cells or more. Figure (1), shows the CFD variation of the total pressure ratio with the number of computational cells.

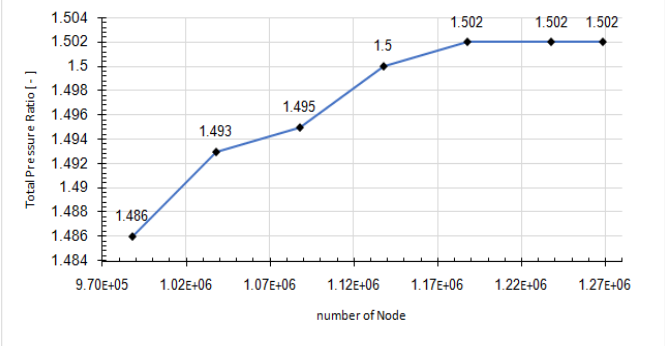

Figure 1: Mesh Independence Study

3. Three Dimensional CFD Results and Discussion

The three-dimensional computational domains are generated from the geometrical parameters determined by the meanline scheme. The impeller blade profile is constructed such that the inlet and outlet blade angle values are connected by a Bezier fitting equation.

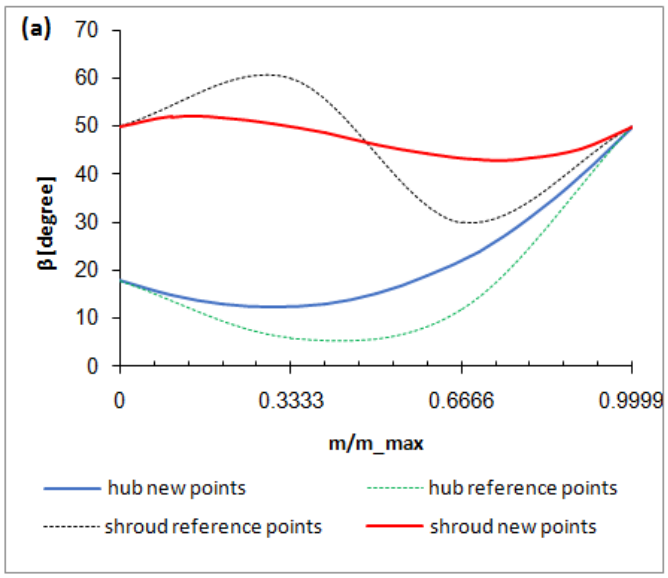

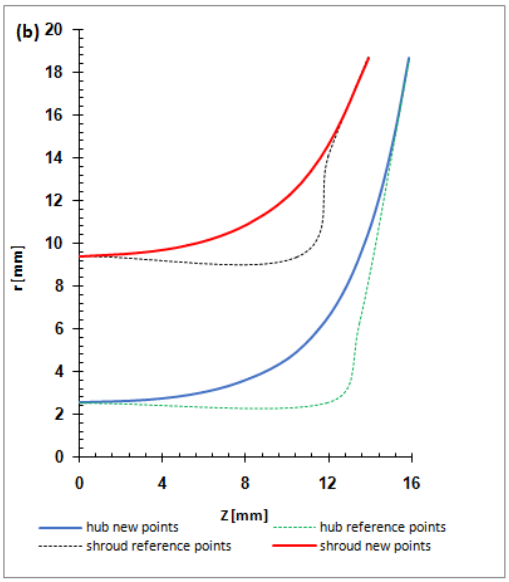

Figure 2: The Impeller Constructed by Bezier Polynomials: (a) Impeller Blade Angles Distribution for the Hub (blue) and Shroud (red) from Inlet to Outlet and (b) Curve Profile of Hub (blue) and Shroud (red) in Meridional Plane

Similarly, the hub and shroud profiles are constructed by connecting the inlet and outlet values, which are determined by the meanline scheme using the Bezier fitting equation[14], [15] (see figure 2 - a and b). The following sections are constructed to cover the validation of the CFD results and the evolution of SCO2 thermophysical and kinematic properties in streamwise, spanwise, and angular directions.

Validation

The CFD results of this study are validated using available experiment data from SNL [7], [16]. The pressure ratio of the CFD cases (CVD1 to CVD12) are compared with experiments as shown in figure (3). The average relative error is found to be 2.3296%. The minimum and maximum relative errors are 0.5396% and 4.688%, respectively. CFD simulation of SCO2 is known as a complicated problem due to the significant change in fluid molecular and transport properties as the pressure and temperature build up. Therefore, the CFD and experimental results are in good agreement, and the relative error is deemed satisfactory (see Table 1)).

Table 1: Validation of CFD results with SNL experimental data

	Rotational speed	Total inlet temperature	Total inlet pressure	Mass flow rate	Pressure ratio		Relative error
	N	T_{01}	P_{01}	$\dot{m}$	Π		ε_r
Cases	(rpm)	(K)	(MPa)	(kg/s)	Exp.	CFD	(%)
CVD1	10000	305.5	7.676	0.454	1.039	1.014	2.406
CVD2	20000	305.5	7.676	0.771	1.051	1.059	0.761
CVD3	28000	305.5	7.676	1.134	1.112	1.118	0.539
CVD4	29888	306.78	7.92	1.315	1.082	1.113	2.865
CVD5	39000	305.6	7.711	1.451	1.204	1.230	2.159
CVD6	49000	306.3	7.854	1.816	1.355	1.325	2.214

International Research Journal of Innovations in Engineering and Technology (IRJIET)
ISSN (online): 2581-3048
Volume 6, Issue 3, pp 13-23, March-2022
https://doi.org/10.47001/IRJIET/2022.603003

CVD7	55000	306.4	7.890	2.043	1.439	1.428	0.764
CVD8	56000	306.6	7.826	2.088	1.469	1.421	3.267
CVD9	59584	308.33	8.224	2.609	1.365	1.429	4.688
CVD10	60000	306.9	7.997	2.225	1.518	1.495	1.515
CVD11	64384	308.71	8.286	2.86	1.441	1.502	4.233

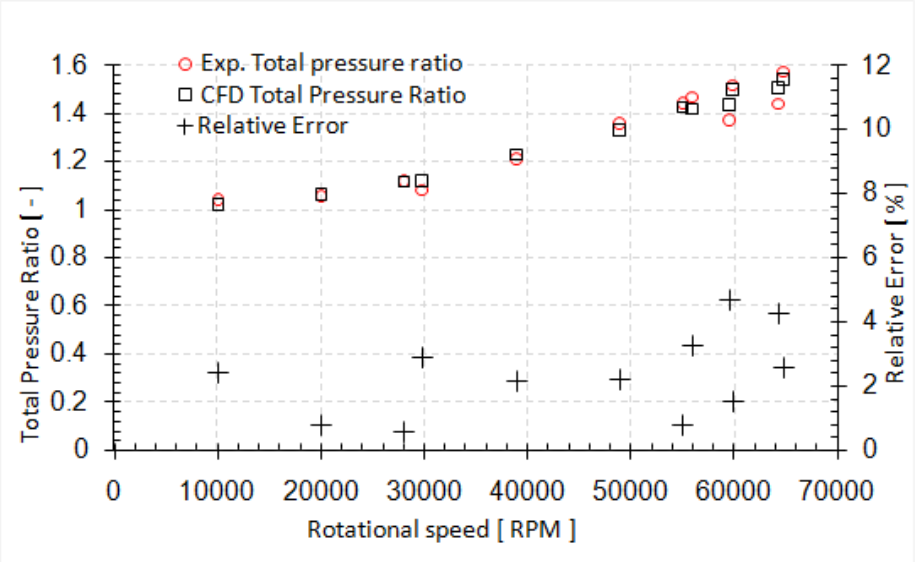

Figure 3: The pressure ratio of the CFD cases (CVD1 to CVD12) are compared with experiments and relative error

Pressure Build up History

The main duty of a centrifugal compressor is to increase the gas pressure of the fluid passing through its rotating impeller, which is required in many industrial applications. In figure (4), the SCO_2buildup develops in both the impeller and the vaned diffuser. The rate at which pressure increases in the impeller is, however, much higher than in the vaned differ. The SCO_2 pressure is elevated by adding kinetic energy, which is projected by accelerating the SCO_2 velocity as it passes through an impeller. The gas potential energy (static pressure) increases when the SCO_2 velocity decelerates at the impeller outlet and as it flows through the diffuser. Figure (5-a, b and c) shows the pressure contour developed at span 50% for the design conditions described in the cases (CVD2, CVD7 and CVD10).

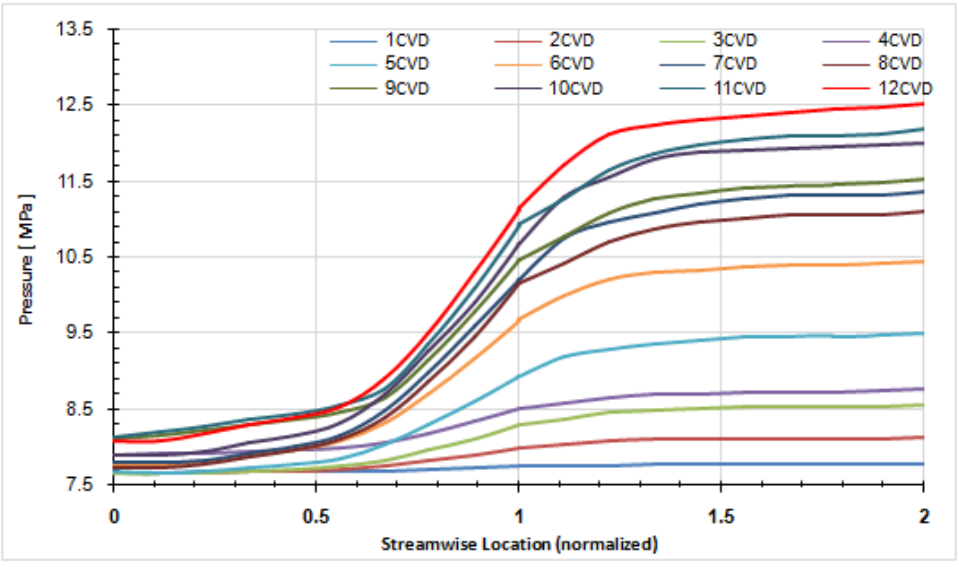

Figure 4: Pressure build up from inlet to outlet for (CVD1 to CVD12)

International Research Journal of Innovations in Engineering and Technology (IRJIET)
ISSN (online): 2581-3048
Volume 6, Issue 3, pp 13-23, March-2022
https://doi.org/10.47001/IRJIET/2022.603003

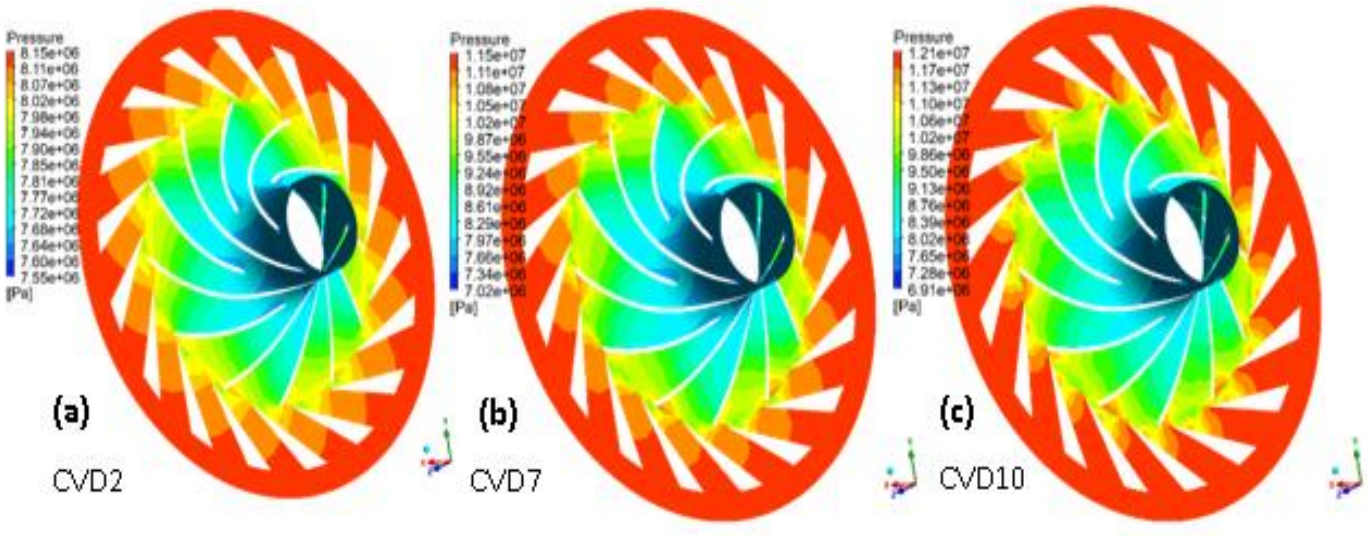

Figure 5: Pressure contour at span 50% for the design conditions described in cases (CVD2, CVD7 and CVD10)

Flow Dynamics

The complex geometry of impeller and diffuser induces complicated flow structure which is characterized by nonlinear three-dimensional, unsteady, high turbulent intensity, and non-stationary frame of reference. In the last thirty years, the CFD tools and computer hardware has significantly improved which enable researchers to explore the flow dynamics in the impeller passage. The CFD flow dynamics provides important information to diagnose regions of high losses in which the flow recirculates. This has crucial importance in design optimization by modifying geometrical parameters to avoid vortical flow and regions high entropy generation. As the fluid enter the impeller, the flow accelerates by virtue of momentum exchange with the rotating impeller blades. Figure (**6**-a and b) shows velocity contour developed at span 50% for the design conditions described in cases CVD1 and CVD12 , respectively . The velocity magnitude varies from 17.9 to 138 m/s as the impeller speed changes from 10000 to 64900 rpm. The flow velocity accelerates faster on the suction side than on the pressure side of both splitter and main blade. A circulation flow is observed in the region next to the trailing edge of vaned diffuser blades. This is due to relatively thick blade at the trailing edge which produces wakes region behind and for all design conditions under consideration.

The vortical flow is considered as losses in which the energy being taken from the mean flow drives the vortical flow. It can be confirmed from pressure contours shown in figure (5) that the rate of pressure increase at the wake region is minimal. Similar observation was found for air compressor [17].In general, for all design conditions, the flow structure through impeller is found to be streamed at span 50% and only small regions of circulation flow observed at the suction side of the main blade in some cases such as CVD2, CVD5, and CVD6 which can be viewed more clearly in figure (**6**-c, d and e).This means that the blade profile is design to fulfill the operating conditions. Figure (**6**–a and b) illustrate the flow velocity contour from hub to shroud at spans 25% and 99% for CVD1. A considerable change in fluid properties can be seen through span wise direction. Near the hub region at span 25%, the flow is streamed, and no flow circulation is observed through impeller passage. In diffuser region, the wake region behind the trailing edge and near leading edge at the pressure side develop vortical flow near hub surface.

The flow structure is, however, exhibits different behavior at higher span ratios. At span 90%, the flow is no longer streamed and vortical flow dominates the passage domain of the impeller. This is attributed to two main reasons; the first is the secondary flow effect caused by tip clearance which allows the flow to pass from pressure to suction sides and hence disturbs the mean flow in the passage near the shroud surface. The second is the fact that the blade speed is maximum at shroud region which contributes to flow turbulent structure. Figure *7*-b) at span 99% clearly shows the SCO_2 flow passes from pressure to suction side over the blades through the tip clearance. The pressure difference between two sides of blade is the driving force of this flow which is generally known as a secondary flow that reduces the performance of the compressor, and that is due to re-circulation of flow of fluid from outlet to inlet through the tip clearance between the impeller and shroud as shown in figure (8 – a and b).

International Research Journal of Innovations in Engineering and Technology (IRJIET)

ISSN (online): 2581-3048

Volume 6, Issue 3, pp 13-23, March-2022

https://doi.org/10.47001/IRJIET/2022.603003

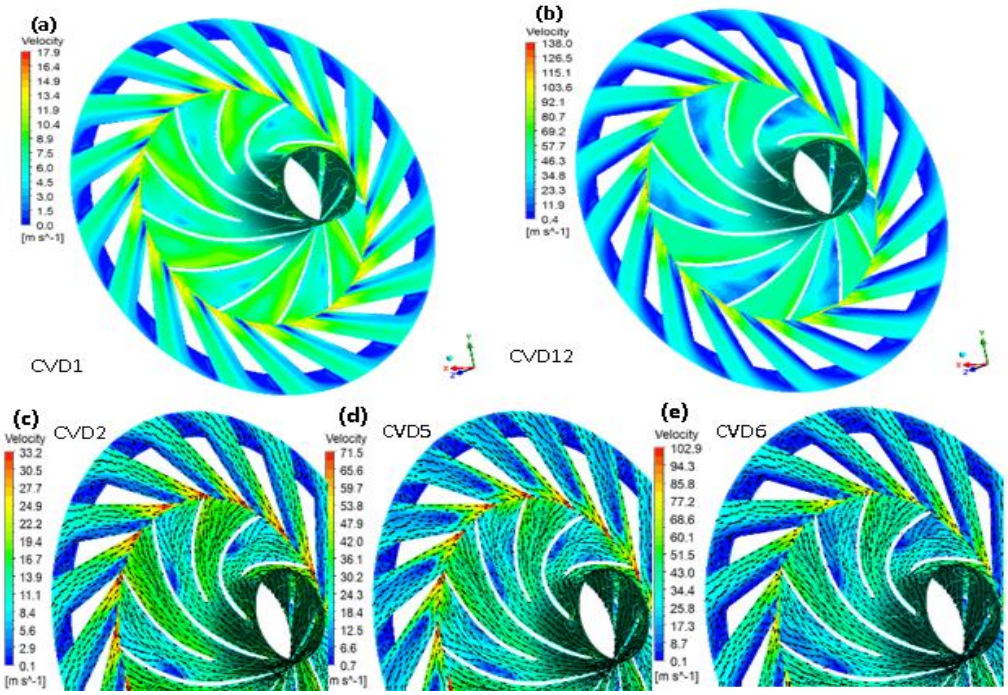

Figure 6: velocity contour and vector at span 50% for selected cases

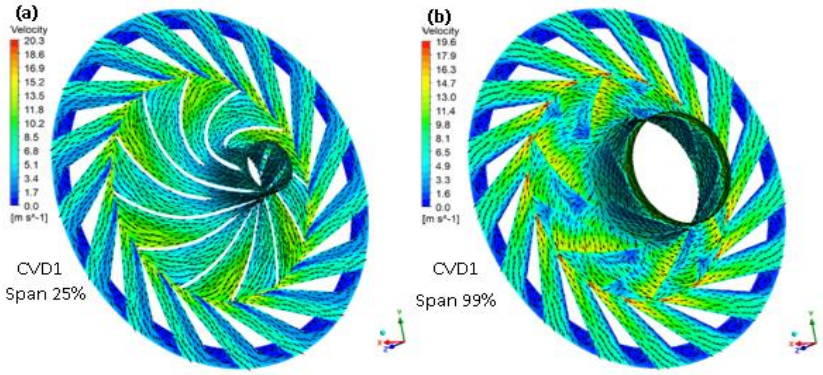

Figure 7: velocity vector for CVD1 at span (a-25% and b- 99%)

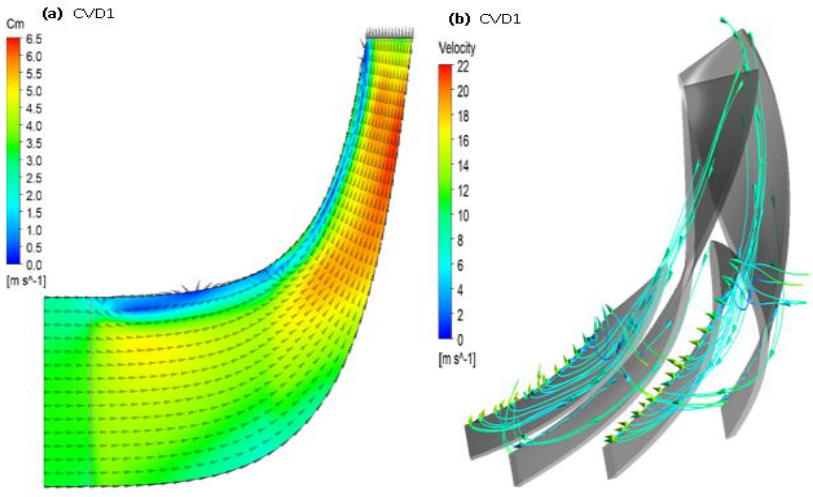

Figure 8: Effect the tip clearance on flow: (a)vector of meridional velocity on meridional surface view and (b)stream velocity over blade through tip clearance

International Research Journal of Innovations in Engineering and Technology (IRJIET)

ISSN (online): 2581-3048

Volume 6, Issue 3, pp 13-23, March-2022

https://doi.org/10.47001/IRJIET/2022.603003

Variation in Thermophysical Properties

Figure (9) demonstrates that the thermophysical properties of SCO_2 present noticeable variation across both spanwise and angular directions. The fluid density reveals highly nonlinear behavior. At the impeller entrance, the temperature is minimum at the suction side and gets close to its critical value. The fluid density, however, shows the highest values even though the pressure is minimal. This deviates from the ideal gas case and can only be seen when the fluid is in the supercritical domain. As the flow moves downstream and its temperature increases and deviates from its critical point, the density starts to decrease. A local increase in fluid density can be seen on the pressure side, at which the SCO_2 fluid experiences a local increase in both pressure and temperature.

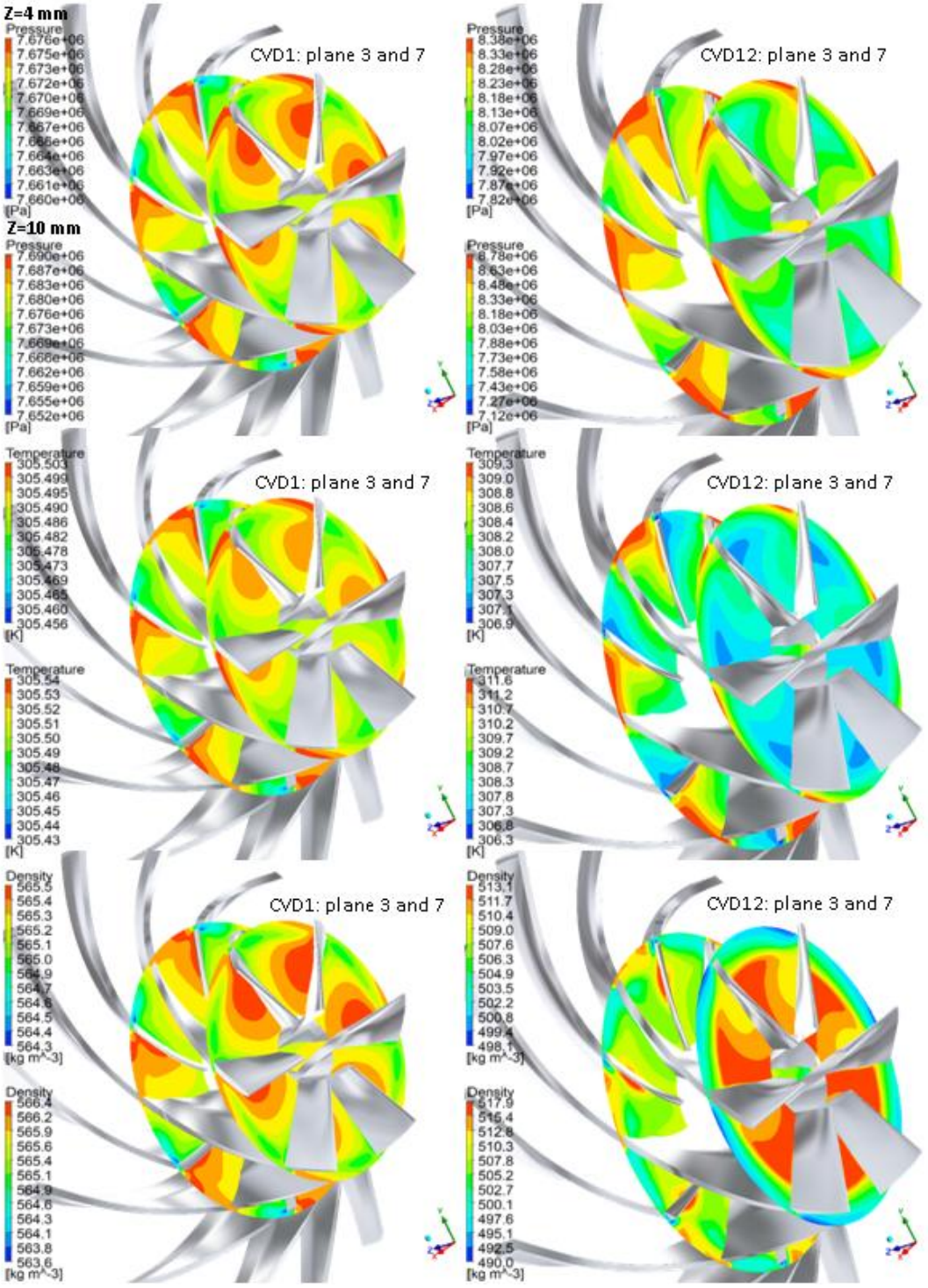

Figure 9: Variation in thermophysical properties of SCO_2

International Research Journal of Innovations in Engineering and Technology (IRJIET)

ISSN (online): 2581-3048

Volume 6, Issue 3, pp 13-23, March-2022

https://doi.org/10.47001/IRJIET/2022.603003

Evolution of Fluid Density

The density of real gas SCO_2 reveals an interesting physics behind the behaviour of SCO_2 when it is brought to a supercritical region. The density of carbon dioxide at standard conditions is of the order of1.98 kg/m^3 and it dramatically increases up to 600 kg/m^3 at supercritical regions. This means that the density increases by 300 times its standard value. Similarly, for the same mass flow, the volume occupied by carbon dioxide in the supercritical region is equivalent to 0.3 percent of that in standard conditions, which hence requires less compression work. Therefore, the supercritical Brayton power cycle is characterized by smaller equipment sizes and plant footprints, and lower capital costs[1].

This behavior imposes considerable challenges to CFD analysis of the centrifugal compressor in which the SCO_2 with a density of 60% of the water density is being compressed to a pressure ratio up to 1.5. The CFD solver is very sensitive to the fluid density, which varies significantly with temperature and pressure at the supercritical region. Therefore, CFD studies using supercritical fluid in a compressor are still marginal[18].

In figure (**10**) the density contours of selected cases are presented. It can be seen that the density change of SCO_2 is nonlinearly correlated with pressure. For example, in case CVD12, the density increases from inlet to outlet by about 85 kg/m^3. The results also confirm the nonlinear behavior of the fluid density evolution in the compressor passage.

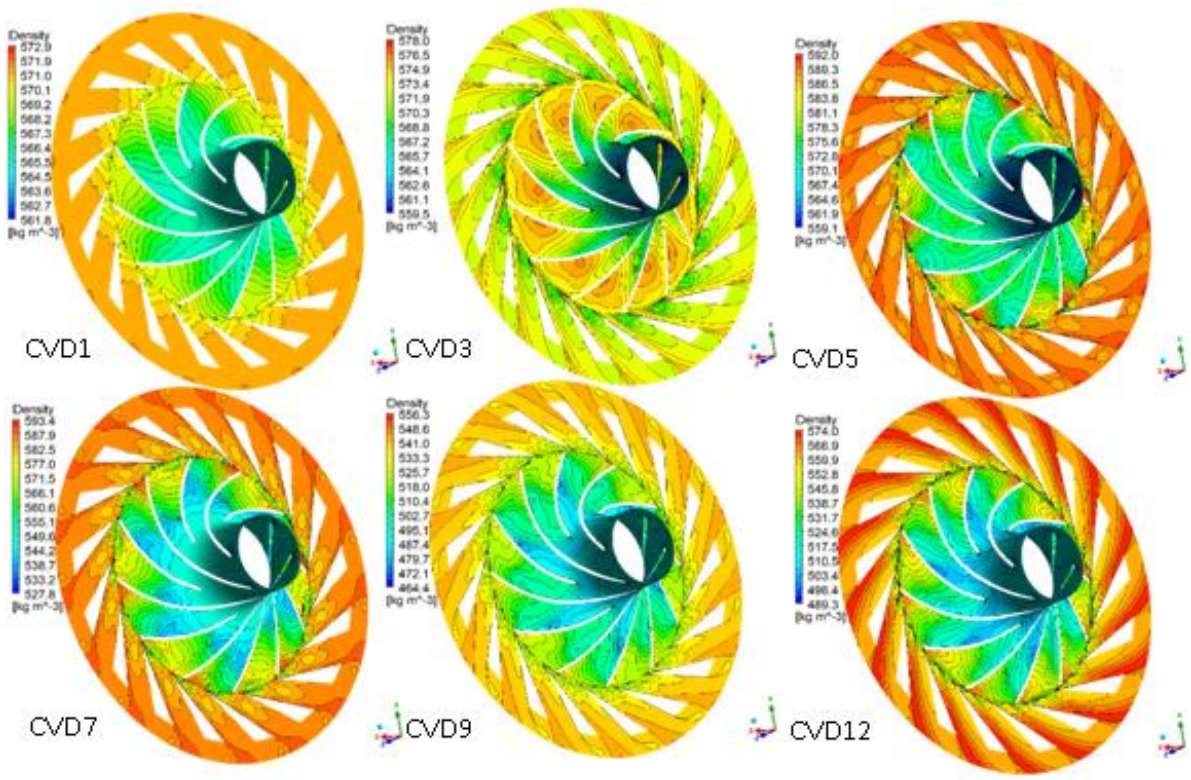

Figure 10: Density contour span 50% for selected cases

Temperature felid

Although the real gas behavior of SCO_2 deviate from that of an ideal gas, the temperature field is controlled by pressure and density. The temperature of the flow increases with the pressure as the flow moves from the inlet to the outlet (see figure (**11**)). The maximum temperature obtained by CFD simulations is observed at the outlet of the case CVD11 as expected since the total inlet temperature is maximum at this case. The temperature gradient follows similar behavior to the rate at which the pressure increases.

On the other hand, the temperature rise can be attributed to the analysis based on total enthalpy which can be assumed as constant in the isentropic case. Here, the static enthalpy is approximately equivalent to the total enthalpy subtracted by the term

International Research Journal of Innovations in Engineering and Technology (IRJIET)

ISSN (online): 2581-3048

Volume 6, Issue 3, pp 13-23, March-2022

https://doi.org/10.47001/IRJIET/2022.603003

($\frac{C^2}{2}$). Since the velocity at the entrance of the impeller accelerated result in decrease of the static enthalpy. However, the flow decelerated at the impeller outlet and through vaned diffuser which cases rise in static enthalpy and hence the temperature.

It should be mentioned here that the SCO_2 compressor develops lower temperature rise than the compressor carbon dioxide in standard condition. This is due to the increase in the specific heat which allows SCO_2 to absorb more heat energy at the same mass flow and temperature difference.

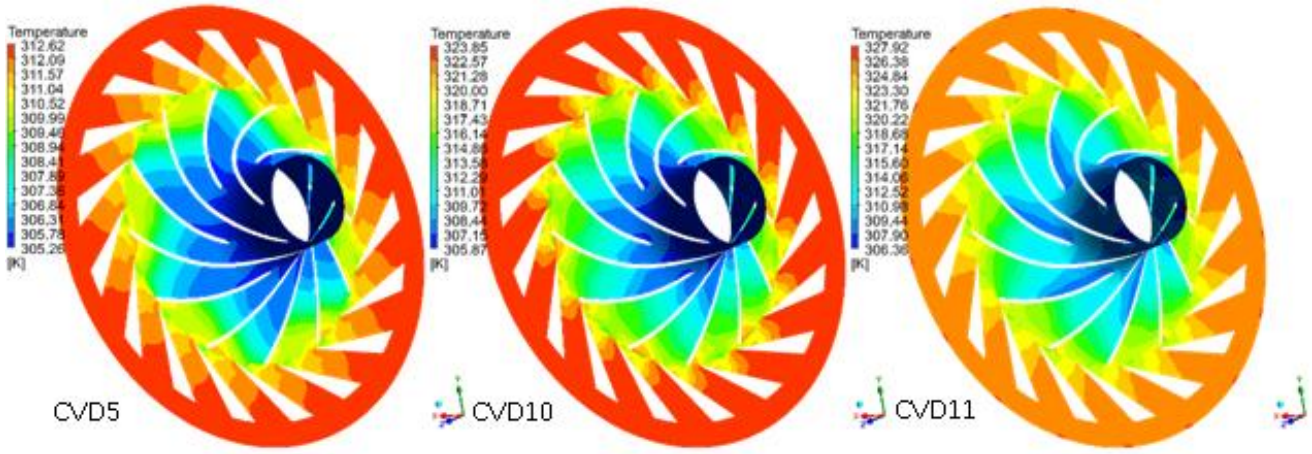

Figure 11: Temperature contour span 50%for selected cases

4. Conclusions

In this work, a meanline code was developed to regenerate one-dimensional analysis of a centrifugal compressor working on a real gas of supercritical CO_2. The analysis includes main geometrical parameters and flow at boundary conditions such as total pressure and temperature at the inlet and mass flow rate at the outlet. Other fluid kinematic and molecular properties are also considered in their evolution. To generate the three-dimensional compressor passage, a Bezier polynomial is used to connect the inlet and outlet data, which includes hub, shroud, and blade profiles. Three-dimensional CFD is then applied to get further insight on the flow structure, secondary flow, and evolution of the thermophysical properties in all directions within the computational domain, which is an essential step to optimize the compressor performance. The supercritical CO_2 is modelled as a real gas using the REFPROP database for both meanline and CFD analysis. It should be stressed here that the twelve cases chosen in this study are applied to the Sandia National Lab. experiment for the sake of comparison. Several conclusions may be drawn from this work as follows:

1. The pressure ratio increases with impeller speed and SCO_2 mass flow rate as it can be concluded from results of CVD1 to CVD3.
2. Flow circulation is observed in case CVD5 at 50% of the span and continues till the span reaches 99% at the suction side of the main blades due to the back flow in the tip clearance region as well as the blockage effect.
3. An interesting behavior of SCO_2 is revealed by CFD results where the density it dramatically increases up to 600 kg/m^3 when it brought to near critical region. This means that the density increases by 300 times its standard value. Similarly, for the same mass flow, the volume occupied by carbon dioxide in the supercritical region is equivalent to 0.3 percent of that in standard conditions, which hence requires less compression work. The results also confirm the nonlinear behavior of the fluid density evolution in the compressor passage. Also, the increase in the density of SCO_2 is affected by the temperature and how close the operating conditions are to the critical point.
4. Entropy increases at suction side and wake region behind the trailing edge of the vanned diffuser blades where losses is considered remarkable, and the flow tends to have vortical structure with high turbulent intensity. The entropy is, however, show minimal values at pressure side of both splitter and main blade where the flow is streamed and aligned with the meridional passage.
5. The three-dimensional CFD results showed good agreement with the experiments data. The average relative error is found to be 2.3296%. The minimum and maximum relative errors are 0.5396% and 4.688%, respectively.
6. The convergence history curves of the CFD solver draw smooth convergence which indicates that the physics has been consistently set up and boundary conditions match the geometrical and impeller speed which have been developed by meanline analysis.

ISSN (online): 2581-3048
Volume 6, Issue 3, pp 13-23, March-2022
https://doi.org/10.47001/IRJIET/2022.603003

Nomenclature

C	Absolute velocity
I	Rothalpy
P	Pressure
Pr_t	Turbulent Prandtl Number
r	Radius
r	location Vector
R	Local Radius
$\boldsymbol{S}_{ui}$	Momentum Source
$\mathbf{S}_{\text{cfg}}$	centrifugal Force
$\mathbf{S}_{Cor}$	Coriolis Force
t	Time
T	Temperature
$\boldsymbol{U}$	Vector of Velocity $\boldsymbol{U}_{x,y,z}$
u_i	Components of the Mean Velocity Vector
x_i	Coordinates

Greek symbols

ρ	Density
ε_r	Relative Error
μ	Molecular (dynamic) Viscosity
μ_t	Turbulent Viscosity
μ_{eff}	Effective Viscosity
λ	Thermal Conductivity
Π	Pressure Ratio

REFERENCES

[1] K. Brun, P. Friedman, and R. Dennis, *Fundamentals and applications of supercritical carbon dioxide (sCO2) based power cycles*, 1st Editio. Woodhead publishing, 2017.

[2] B. D. Iverson, T. M. Conboy, J. J. Pasch, and A. M. Kruizenga, "Supercritical CO2 Brayton cycles for solar-thermal energy," *Appl. Energy*, vol. 111, pp. 957–970, 2013, doi: 10.1016/j.apenergy.2013.06.020.

[3] C. S. Turchi, Z. Ma, T. W. Neises, and M. J. Wagner, "Thermodynamic study of advanced supercritical carbon dioxide power cycles for concentrating solar power systems," *J. Sol. Energy Eng. Trans. ASME*, vol. 135, no. 4, pp. 1–7, 2013, doi: 10.1115/1.4024030.

[4] V. Dostal, P. Hejzlar, and M. J. Driscoll, "High-performance supercritical carbon dioxide cycle for next-generation nuclear reactors," *Nucl. Technol.*, vol. 154, no. 3, pp. 265–282, 2006, doi: 10.13182/NT154-265.

[5] M. Utamura, T. Fukuda, and M. Aritomi, "Aerodynamic Characteristics of a Centrifugal Compressor Working in Supercritical Carbon Dioxide," *Energy Procedia*, vol. 14, pp. 1149–1155, 2012, doi: 10.1016/j.egypro.2011.12.1068.

[6] R. Pecnik, E. Rinaldi, and P. Colonna, "Computational Fluid Dynamics of a Radial Compressor Operating With Supercritical CO2," in *Volume 5: Manufacturing Materials and Metallurgy; Marine; Microturbines and Small Turbomachinery; Supercritical CO2 Power Cycles*, Jun. 2012, vol. 5, pp. 985–995, doi: 10.1115/GT2012-69640.

[7] S. a Wright, R. F. Radel, M. E. Vernon, G. E. Rochau, and P. S. Pickard, "Operation and Analysis of a Supercritical CO2 Brayton Cycle," *SANDIA Rep. SAND2010-0171*, no. September, p. 101, 2010, [Online]. Available: http://prod.sandia.gov/techlib/access-control.cgi/2010/100171.pdf.

[8] H. Zhao, Q. Deng, K. Zheng, H. Zhang, and Z. Feng, "Numerical investigation on the flow characteristics of a supercritical CO2 centrifugal compressor," *Proc. ASME Turbo Expo*, vol. 3B, pp. 1–10, 2014, doi: 10.1115/GT2014-26646.

[9] A. Ameli, T. Turunen-saaresti, A. Grönman, and J. Backman, "Compressor design method in the supercritical CO2 applications," *6th Int. Symp. - Supercrit. CO2 Power Cycles*, 2018.

[10] S. K. Raman and H. D. Kim, "Computational analysis of the performance characteristics of a supercritical CO2 centrifugal compressor," *Computation*, vol. 6, no. 4, pp. 1–16, 2018, doi: 10.3390/computation6040054.

[11] X. Li, Y. Zhao, H. Yao, M. Zhao, and Z. Liu, "A new method for impeller inlet design of supercritical CO2 centrifugal compressors in brayton cycles," *Energies*, vol. 13, no. 19, 2020, doi: 10.3390/en13195049.

[12] P. E. Smirnov and F. R. Menter, "Sensitization of the SST turbulence model to rotation and curvature by applying the Spalart-Shur correction term," *J. Turbomach.*, vol. 131, no. 4, pp. 1–8, 2009, doi: 10.1115/1.3070573.

[13] Z. A. AL-SUHAIBANI, "FLOW ANALYSIS AND MODELING OF CENTRIFUGAL COMPRESSOR IMPELLERS," Michigan State University, 2005.

[14] M. V. Casey, "A computational geometry for the blades and internal flow channels of centrifugal compressors," *Proc. ASME Turbo Expo*, vol. 1, pp. 1–11, 1982, doi: 10.1115/82-GT-155.

[15] A. R. Forrest, "Interactive interpolation and approximation by Bézier polynomials," *Comput. Des.*, vol. 22, no. 9, pp. 527–537, 1990, doi: 10.1016/0010-4485(90)90038-E.

[16] PhD Candidate: Benjamín Monge Brenes, "Design of supercritical carbon dioxide centrifugal compressors," *Vet. Parasitol.*, p. 169, Mar. 2014.

[17] S. S. Lee Gibson, Lee Galloway, Sung in Kim*, "Assessment of turbulence model predictions for a centrifugal compressor simulation," *J. Glob. POWER Propuls. Soc.*, vol. 133, no. 1, pp. 142–156, 2017, doi: 10.22261/2II890.

[18] Y. Wang, D. Shi, D. Zhang, and Y. Xie, "Investigation

ISSN (online): 2581-3048
Volume 6, Issue 3, pp 13-23, March-2022
https://doi.org/10.47001/IRJIET/2022.603003

on unsteady flow characteristics of a SCO2 centrifugal compressor," *Appl. Sci.*, vol. 7, no. 4, 2017, doi: 10.3390/app7040310.

Citation of this Article:

Firas Khaleel Hussein Alok, Dr. Younis M. Najim, "Three Dimensional CFD of Supercritical CO_2 Flow Characterization in a Centrifugal Compressor" Published in *International Research Journal of Innovations in Engineering and Technology - IRJIET*, Volume 6, Issue 3, pp 13-23, March 2022. Article DOI https://doi.org/10.47001/IRJIET/2022.603003

****

